THE JOURNAL OF PHYSICAL CHEMISTRY Letters

Letter

Cite This: J. Phys. Chem. Lett. 2019, 10, 1482−1488

pubs.acs.org/JPCL

DORI Reveals the Influence of Noncovalent Interactions on Covalent Bonding Patterns in Molecular Crystals Under Pressure

Benjamin Meyer,[†,‡] Senja Barthel,[‡,§,#] Amber Mace,[‡,§,∥,#] Laurent Vannay,[†,#] Benoit Guillot,[⊥] Berend Smit,[‡,§] and Clémence Corminboeuf*[,†,‡]

[†]Laboratory for Computational Molecular Design (LCMD), Institute of Chemical Sciences and Engineering (ISIC), École Polytechnique Fédérale de Lausanne (EPFL), CH-1015 Lausanne, Switzerland

[‡]National Center for Computational Design and Discovery of Novel Materials (MARVEL), École Polytechnique Fédérale de Lausanne (EPFL), CH-1015 Lausanne, Switzerland

[§]Laboratory of Molecular Simulation (LSMO), Institute of Chemical Sciences and Engineering (ISIC), École Polytechnique Fédérale de Lausanne (EPFL Valais), CH-1951 Sion, Switzerland

[∥]Department of Materials and Environmental Chemistry, Stockholm University, SE-10691 Stockholm, Sweden

[⊥]Laboratoire CRM2, UMR 7036, Université de Lorraine, F-54506 Vandoeuvre-lès-Nancy, France

Supporting Information

ABSTRACT: The study of organic molecular crystals under high pressure provides fundamental insight into crystal packing distortions and reveals mechanisms of phase transitions and the crystallization of polymorphs. These solid-state transformations can be monitored directly by analyzing electron charge densities that are experimentally obtained at high pressure. However, restricting the analysis to the featureless electron density does not reveal the chemical bonding nature and the existence of intermolecular interactions. This shortcoming can be resolved by the use of the DORI (density overlap region indicator) descriptor, which is capable of simultaneously detecting both covalent patterns and noncovalent interactions from electron density and its derivatives. Using the biscarbonyl[14]annulene crystal under pressure as an example, we demonstrate how DORI can be exploited on experimental electron densities to reveal and monitor changes in electronic structure patterns resulting from molecular compression. A novel approach based on a flood-fill-type algorithm is proposed for analyzing the topology of the DORI isosurface. This approach avoids the arbitrary selection of DORI isovalues and provides an intuitive way to assess how compression packing affects covalent bonding in organic solids.

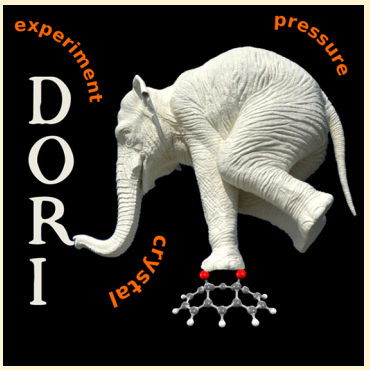

Studies of matter under high pressure have long been the realm of geoscientists, solid-state physicists, and astrophysicists who examine the extreme conditions of Earth[1] and extraterrestrial environments.[2] In materials science, pressure is also exploited to control the properties of materials, for instance, by reducing interatomic or intramolecular distances.[3−6] This leads to a host of interesting applications, ranging from superhard[7,8] and high-energy density materials[9] to hydrogen storage.[10] We are interested in the behavior of molecular organic and metal−organic crystals under pressure.[11−13] Such an understanding provides deep insight into the pressure-induced distortions of crystal packing, the switching of molecular conformations, and the exploration of new polymorphic forms (e.g., chemisorption in metal−organic frameworks,[14,15] piezochromic switches,[16,17] photovoltaic hybrid perovskites,[18,19] the crystal engineering of pharmaceuticals,[20] as well as amino acids[21,22] and sugars[23,24]).

During variable pressure experiments, changes appear in the molecular geometries[25] (e.g., interatomic distances and angles) due to the compression of molecular packing.[26−28] But these geometrical changes do not directly allow the deduction of changes in the electronic structure, which represents perhaps the most appealing and sensitive way of examining inter- and intramolecular interactions of compressed molecular crystals. The ability to experimentally observe electronic structure modifications under pressure is relatively recent.[29−32] Macchi's work on *syn*-1,6:8,13-biscarbonyl[14]annulene (BCA) (see Figure 1) represents a major breakthrough.[33] This BCA crystal was chosen to be studied because its charge density at ambient pressure revealed an unusual bond path that links the two bridgehead carbonyl groups in almost C_{2v} molecular symmetry but shifts toward one of the resonant forms[34] of an ideal aromatic system when high pressure is applied, as shown in Figure 1. Applying pressure weakens the electron delocalization in the double bonds of the annulene ring that is observed at ambient pressure, distorting the systems to the C_s subsymmetry point group of C_{2v}. As for the packing, BCA crystallizes with four molecules in the unit cell, with no change

Received: January 24, 2019
Accepted: March 13, 2019
Published: March 13, 2019

DOI: 10.1021/acs.jpclett.9b00220
J. Phys. Chem. Lett. 2019, 10, 1482−1488

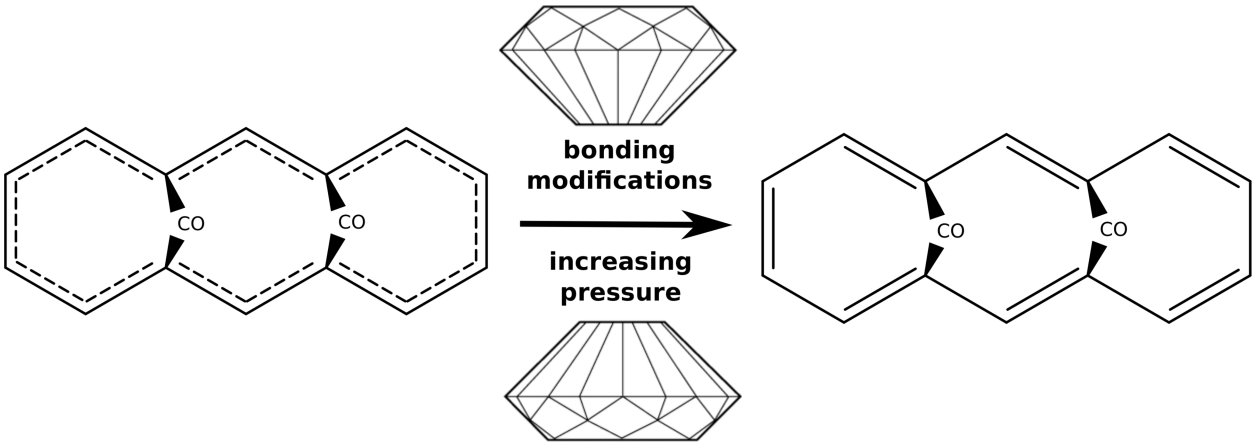

Figure 1. Ideal aromatic representation (left) and resonance structure (right) for the *syn*-1,6:8,13-biscarbonyl[14]annulene (BCA) molecule.

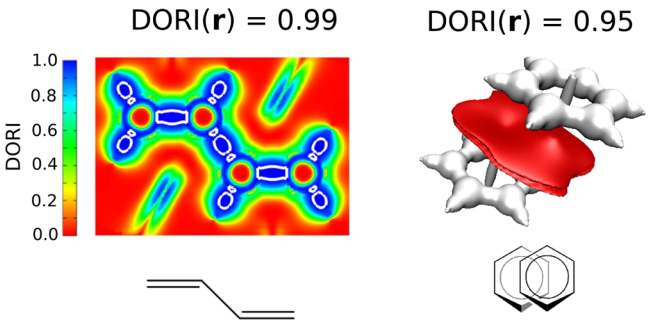

Figure 2. 2D DORI maps (DORI(**r**) = f) in the σ_h plane of butadiene with f = 0.99 isocontour in white (left). 3D representation of the parallel-displaced benzene dimer for f = 0.95 (right) with covalent and noncovalent DORI [f] domains depicted in white and red, respectively. These examples are adapted and reprinted with permission from ref43.

in space group (monoclinic $P2_1/n$) detected when increasing the pressure up to 7.7 GPa.

Whereas the geometric perturbations caused by placing the BCA crystal under pressure are easy to observe, a subtle computational analysis is required to determine the bond type and to illuminate the interplay between chemical bonds and the crystal packing[25] from the experimental electron density.[35] Several methods for analyzing electron charge densities have been proposed in the literature: topological analysis,[36] quantum crystallography,[37] and the use of molecular scalar fields.[38−40] Among the latter, the density overlap region indicator (DORI)[41] (derived from the single exponential decay detector (SEDD)[42]) is a specific and ideally suited example because it reveals both covalent and noncovalent interactions directly from the charge density, $\rho(\mathbf{r})$, (and its derivatives) that is accessible from experiment. DORI is defined as

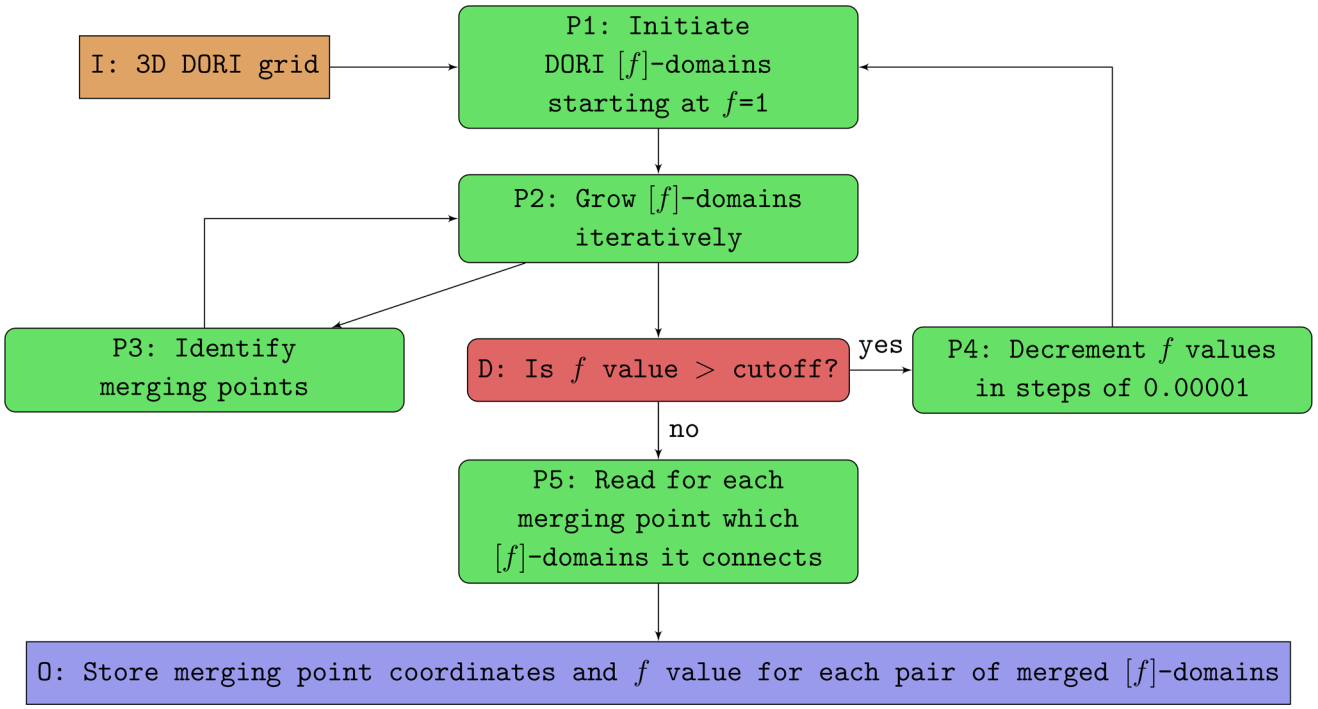

Figure 3. Schematic outline of the search for merging points. The boxes are colored as orange = input (I), blue = output (O), green = processes (P1−P5), and red = decision (D).

DOI: 10.1021/acs.jpclett.9b00220
J. Phys. Chem. Lett. 2019, 10, 1482−1488

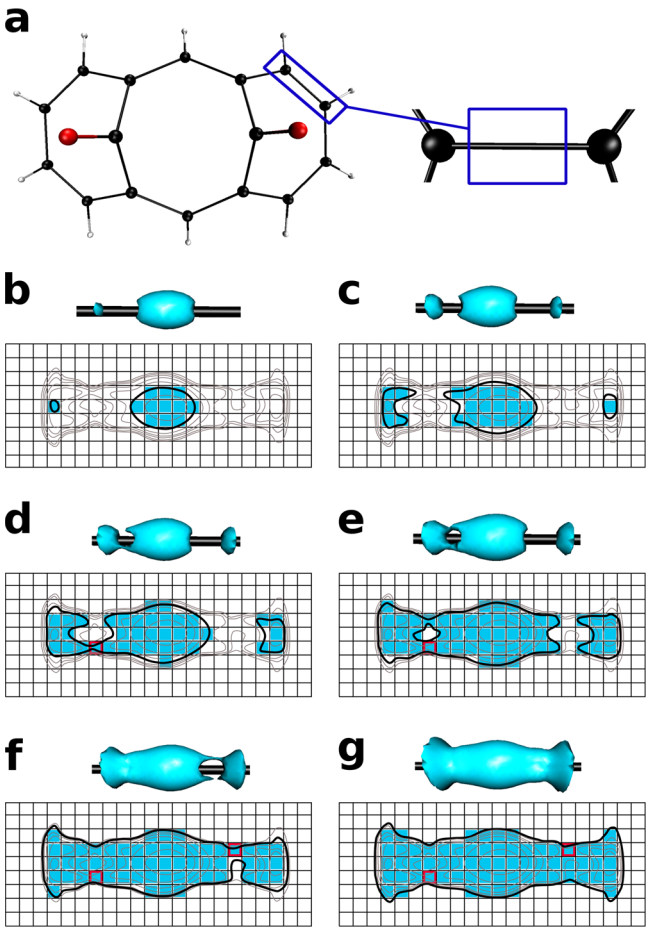

Figure 4. 3D illustration and its schematic 2D analogue of DORI $[f]$ domains for a given C−C bond (a) of BCA at ambient pressure with f = 0.9990 (b), f = 0.9984 (c), f = 0.9980 (d), f = 0.9978 (e), f = 0.9966 (f), and f = 0.9940 (g). The gray lines represent DORI isocontours for each step. For each step, the grid points (in black) with DORI values higher than f are shown in blue. Red encircled grid points correspond to the basin merging points (e.g., three basins merged in two points in panels d and f).

$$\mathrm{DORI}(\mathbf{r}) = \frac{\theta(\mathbf{r})}{1 + \theta(\mathbf{r})} \tag{1}$$

where

$$\theta(\mathbf{r}) = \frac{\left(\nabla\left(\frac{\nabla\rho(\mathbf{r})}{\rho(\mathbf{r})}\right)^2\right)^2}{\left(\frac{\nabla\rho(\mathbf{r})}{\rho(\mathbf{r})}\right)^6} \tag{2}$$

Intuitively, DORI captures the deviations from the single-exponential behavior of the density in real space and reveals density overlaps between atomic shells, atoms, or molecules.[41] The regions of these overlapping charge densities can be directly interpreted as covalent bonds (if the regions lie between atoms) or noncovalent interactions (if the regions lie between molecules).[41] Plotting the DORI values on the 0 to 1 scale leads to unambiguous representations of these overlaps, as shown in Figure 2.

Like any other scalar field on a 3D domain, the representation of DORI requires a fourth dimension (three dimensions for $\mathbb{R}^3$ and one for the value of the function). To visualize the essential features of DORI in three dimensions, one selects a meaningful function value f and displays the closed isosurfaces for f. These surfaces are the boundaries of the $[f]$ domains (i.e., the points with $\mathrm{DORI}(\boldsymbol{r}) = f$), where $[f]$ domains are all points in space with the DORI value greater than or equal to the chosen isovalue f (i.e., the points with $\mathrm{DORI}(\mathbf{r}) \geq f$)). The DORI basins correspond to chemical interactions, which can be quantified by integrating the electron density that is enclosed in each basin

$$DORI(\mathbf{r})_{\mathrm{int}}(V_{[f]}) = \int_{V_{[f]}} \rho(\mathbf{r})\, \mathrm{d}r \tag{3}$$

Noncovalent interactions and bonding patterns are then directly compared using the integral of the electron density ($\mathrm{DORI}(\mathbf{r})_{\mathrm{int}}$) and the volume of the DORI basins ($V_{[f]}$). However, as evident from eq 3, the size and even the number of DORI basins directly depends on the chosen f value. Lowering f, for instance, results in the merging of previously distinct domains. This type of behavior has been rationalized by Savin and Marx,[44] who used bifurcation diagrams to depict maxima and saddle points (the points where basins occur and merge) for the electron localization function (ELF). Heuristic examinations of these bifurcation diagrams have led to a more comprehensive picture of covalent bonding in alkene,[45] aromatic,[46] and biologically relevant[47] systems. However, the bifurcation points (of ELF) were never automatically detected using an algorithmic approach.

Up to now, we generally considered two or three distinct f values to ensure the robustness of any observation of trends associated with DORI fingerprints.[41,43] Such arbitrary choices are, in the best case, nonideal and, in the worst case, may lead to inaccurate conclusions. Picking a single DORI-f value would be especially inconsistent when the experimentally measured electron density is obtained under different thermodynamic conditions (e.g., pressure and temperature) and is therefore not one-to-one comparable. Here we overcome the arbitrariness of selecting DORI isovalues by exploiting an algorithm that continuously and automatically monitors the DORI basins and the positions of their merging points while decreasing the f value. Taking the average of the DORI-f values of all of the bond merging points gives a meaningful and unique choice of the f value at which the covalent bonds are analyzed. This uniqueness together with the ability of DORI to simultaneously reveal covalent and noncovalent regions provides a breakthrough in assessing how high pressure affects the peculiar interplay between bonding patterns and compression packing.

Inspired by the idea of the bifurcation diagram but adopting an algorithmic approach, we analyzed the BCA covalent bonding pattern under ambient and high pressure using a connected component search algorithm[48] (see Figure 3). The algorithm performs a topological analysis of the DORI function based on 3-manifold decomposition theory and identifies its critical points (e.g., maxima and saddle point; see the details in the Supporting Information). A similar algorithm has recently been applied to study methane diffusion in nanoporous materials from a potential energy field.[48] In short, while decreasing the DORI values, the connected component search algorithm lists the coordinates of the grid points belonging to the growing DORI $[f]$ domains and detects the merging points (i.e., both their DORI values and their coordinates) between any pair of different basins.

DOI: 10.1021/acs.jpclett.9b00220
J. Phys. Chem. Lett. 2019, 10, 1482−1488

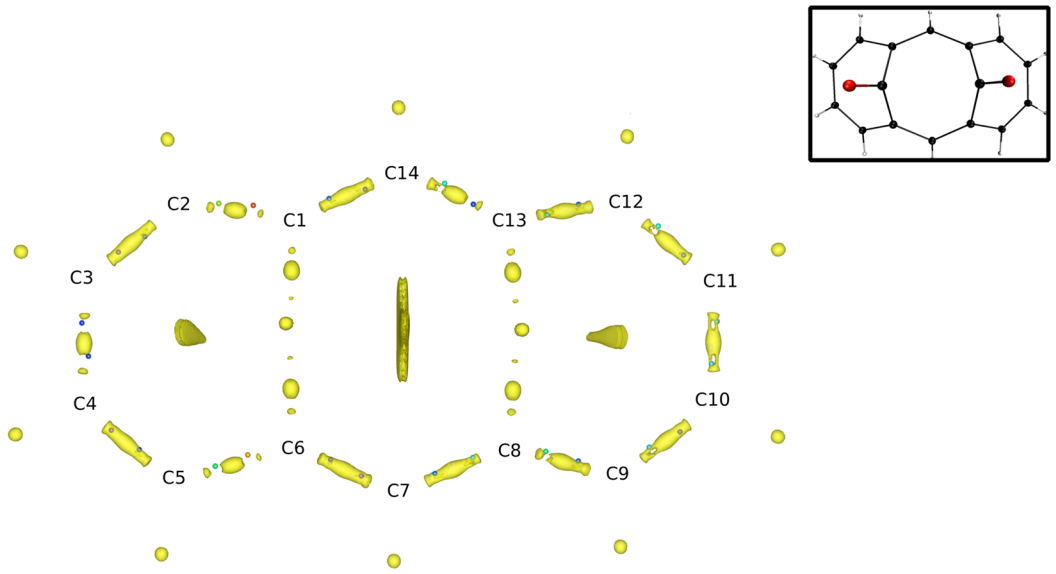

Figure 5. DORI isosurface (DORI(**r**) = f) of BCA at high pressure is shown for f = 0.999 with 28 detected merging points associated with the 14 covalent C−C bonds. Each carbon−carbon bond can be assimilated to three growing basins (e.g., between C1 and C2) that merge into one (e.g., between C10 and C11). The first point that connects two basins is selected as their merging point. The top-right corner is a reminder of the underlying BCA molecule.

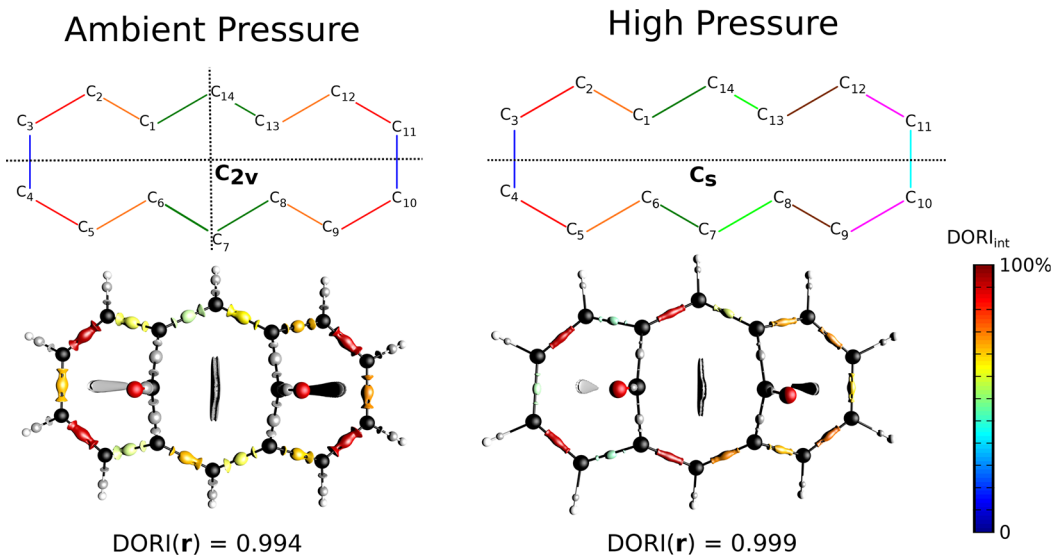

Figure 6. Annulene skeleton at the experimental symmetries: C_{2v} very close to the configuration at ambient pressure (top left) and one of the C_s subsymmetry close to the molecule in the crystal at high pressure (top right). DORI basins of each C−C bond are color-coded to represent the relative percentage of the electron density integrals ($DORI_{int}$) within the basins (relative to the maximum found) at ambient (bottom left) and high pressure (bottom right). All integral values ($DORI_{int}$) and volumes of the basins ($DORI_{vol}$) are given in the Supporting Information.

Figure 4 provides a schematic illustration of the algorithm on a BCA C−C bond. The volume of the DORI domains (in blue) associated with the bond increases with decreasing DORI-f until the merging occurs (visible in red). This covalent bond is properly captured at DORI-f values, for which the three basins defining this bond are merged into one basin. Because the annulene ring of the BCA is composed of 14 C−C bonds, the value used to study the pressure-induced bonding modifications corresponds to the average f value of the 28 merging points (see Figure 5, DORI(**r**) = 0.994 and DORI(**r**) = 0.999 isovalues for the ambient and the high-pressure conditions; all merging point's DORI-f values are provided in the Supporting Information).

With 14 conjugated carbon atoms, the BCA annulene backbone is pseudo-Hückel aromatic ($4n$+2 π electrons) with a distortion from planarity imposed by the two carbonyl bridges.[49] Under ambient conditions, BCA has an experimentally verified C_{2v} symmetry.[50] In Figure 6 (where the basins are colored proportionally to the maximum $DORI_{int}$ found under each condition), the insight obtained from the DORI domains goes beyond geometrical effects. DORI captures the "electronic" equivalence of the bonds that is imposed by the symmetry. At high pressure, the additional stress perturbs the BCA electron delocalization and distorts the electron density of the annulene electron skeleton. This results in an inhomogeneous contraction of the C−C bonds reflected by the drastic changes in the DORI covalent patterns. (All

DOI: 10.1021/acs.jpclett.9b00220
J. Phys. Chem. Lett. 2019, 10, 1482−1488

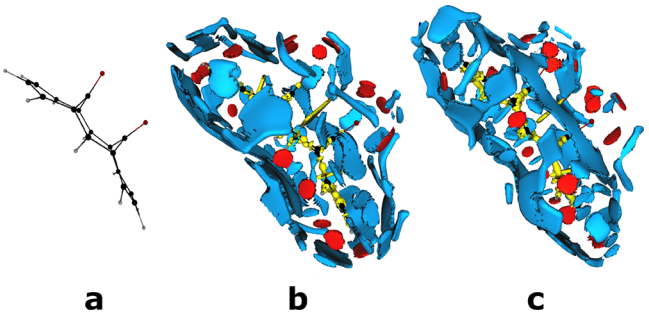

Figure 7. (a) BCA geometry. Noncovalent (DORI(**r**) = f) domains of a single BCA molecule in (b) an ambient and (c) a high-pressure crystal environment. van der Waals interactions are colored in blue, CH···O in red, and covalent bonds in yellow. f = 0.994 and 0.999 for ambient and high pressure, respectively.

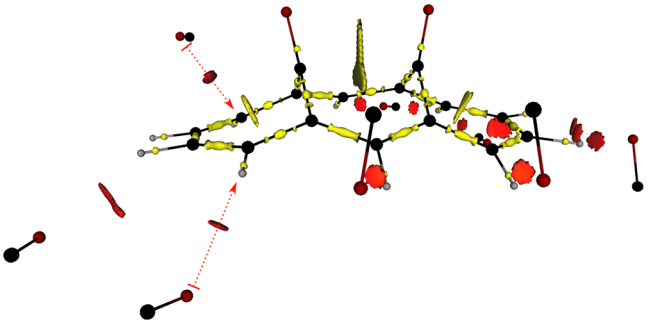

Figure 8. DORI = 0.999 isosurfaces associated with the CH−O interactions of a BCA molecule in a crystal environment at high pressure. Red arrows indicate out-of-plane interactions.

$DORI_{int}$ and $DORI_{vol}$ are given in the Supporting Information.) In particular, as attested by the electron density integrated within the DORI [f] domains (i.e., $DORI_{int}$), the left side of the molecule shows an alternation between compressed (e.g., C1−C14, C2−C3, C4−C5, C6−C7) and loose (e.g., C2−C1, C5−C6) bonds, whereas the right side maintains a partial electron delocalization and smaller electronic compression of the C−C bonds (see Figure 6). Those observations are in line with other indicators (e.g., electron density at the bond critical points,[36] delocalization indices,[51] and extremely localized molecular orbitals[52]) and with quantum-chemical computations (see comparisons with gas-phase and periodic density functional theory (DFT) computations in the Supporting Information). The electron density measured at high pressure integrated within the DORI [f] domains attests to the charge density accumulation in specific bonds of the annulene ring (see Figure 6), which desymmetrizes the molecule. DORI, however, has the advantage of giving a more intuitive visual picture of the pressure-induced modifications of the covalent pattern using an experimental electron density as the sole ingredient.

More relevantly, DORI not only captures the symmetry break and the charge-density accumulation but also identifies their cause, which lies in the distinct packing environment on the left and right sides of the BCA. Whereas the fact that high-pressure crystal packing would somehow induce an anisotropy within the π-conjugation covalent pattern is rather intuitive,[25,53] only indirect measurements of this phenomenon based on two photon spectroscopy[54,55] or geometrical parameters[23,24,56,57] have been observed. The cause and effects are here revealed directly and unambiguously.

At ambient pressure, DORI captures a rich network of noncovalent interactions around a single BCA molecule (see Figure 7) and distinguishes between CH···O interactions, pseudo $\pi-\pi$ stacks, and hydrogen contacts. The seven nonredundant CH···O interactions experimentally characterized in the BCA crystal[50] are reflected by the directional DORI domains (see red basins in Figure 7), typical for hydrogen bonding.[41] (Integral values, $DORI_{int}$, and volume of the basins, $DORI_{vol}$, are given in the Supporting Information.) Many nondirectional van der Waals regions that span all around each BCA at ambient and high pressure are also clearly visible in blue. The monitoring of this noncovalent network upon compression discloses which interactions cause the largest changes in the covalent bonding patterns.

The rearrangement of directional interactions (e.g., OH···O, NH···O, and CH···O bonds or O···O contacts) is especially essential to interpret the modifications of compressed molecular crystals.[23,24,56,57] From the DORI viewpoint, the CH···O bridges are the key to rationalize the BCA covalent pattern. As pressure is applied, several CH···O DORI domains slide from the typical CH···O to the unconventional $\begin{smallmatrix}C\\|\\H\end{smallmatrix}\cdots O$ contact, where the interacting basin now points to the carbon−hydrogen bond. In particular, two of these interactions occur out of the pseudoplane of BCA, pushing the neighboring carbon atom forward (see Figure 8). The C2 and C5 carbon atoms involved in those noncovalent contacts are both located in the same seven-membered ring (C1−C2−C3−C4−C5−C6−C15), explaining the stronger bond length alternation in the left part of the molecule. The right side of the BCA molecule is involved in strong CH···O contacts that remain in the annulene plane, disturbing the C−C covalent patterns to a lesser extent. At even higher pressure, we can expect those interactions to slide out of the pseudoplane, disturbing the symmetry on both sides.

In summary, we analyzed the experimental electron densities of the BCA crystal under high pressure and demonstrated how DORI intuitively captures the dramatic effects of noncovalent interactions on bonding patterns. Our approach relies on a connected component search algorithm, which avoids the arbitrary selection of the DORI isovalue and provides a general framework for the cause−effect analysis of electronic structure patterns in molecular crystals under pressure or under any distinct (e.g., temperature, condensed environment) conditions.

■ ASSOCIATED CONTENT

Supporting Information

The Supporting Information is available free of charge on the ACS Publications website at DOI: 10.1021/acs.jpclett.9b00220.

Details of the electron density refinement and of the flood-fill-type algorithm, all merging points of covalent [f] domains, volume and integral of the electron density within covalent and noncovalent DORI [f] domains, and additional 2D and 3D DORI representations (PDF)

■ AUTHOR INFORMATION

Corresponding Author

*E-mail: clemence.corminboeuf@epfl.ch. Tel: +41 (0)21 693 93 57. Fax: +41 (0)21 693 97 00.

DOI: 10.1021/acs.jpclett.9b00220
J. Phys. Chem. Lett. 2019, 10, 1482−1488

ORCID

Senja Barthel: 0000-0002-9175-5067
Amber Mace: 0000-0002-0323-0210
Berend Smit: 0000-0003-4653-8562
Clémence Corminboeuf: 0000-0001-7993-2879

Author Contributions

#S.B, A.M., and L.V. contributed equally to this work.

Notes

The authors declare no competing financial interest.

■ ACKNOWLEDGMENTS

This work has been supported by EPFL and the National Centre of Competence in Research (NCCR) Materials Revolution: Computational Design and Discovery of Novel Materials (MARVEL) of the Swiss National Science Foundation (SNSF). S.B. and B.S. are supported by the European Research Council (ERC) under the European Unions Horizon 2020 research and innovation program (grant agreement no. 666983, MaGic). A.M. thanks the Swedish Council (VR) for financing (project number 2015-06320). This work was supported by a grant from the Swiss National Supercomputing Centre (CSCS) under project ID s761. We thank Ganna Gryn'ova for the graphical content. We thank Piotr de Silva for his past contribution and discussions associated with DORI.

■ REFERENCES

(1) Ohta, K.; Kuwayama, Y.; Hirose, K.; Shimizu, K.; Ohishi, Y. Experimental Determination of the Electrical Resistivity of Iron at Earth's Core Conditions. *Nature* **2016**, *534*, 95−98.

(2) Rozel, A. B.; Golabek, G. J.; Jain, C.; Tackley, P. J.; Gerya, T. Continental Crust Formation on Early Earth Controlled by Intrusive Magmatism. *Nature* **2017**, *545*, 332−335.

(3) Zhang, L.; Wang, Y.; Lv, J.; Ma, Y. Materials Discovery at High Pressures. *Nat. Rev. Mater.* **2017**, *2*, 17005.

(4) Hemley, R. J. Effects of High Pressure on Molecules. *Annu. Rev. Phys. Chem.* **2000**, *51*, 763−800.

(5) Grochala, W.; Hoffmann, R.; Feng, J.; Ashcroft, N. The Chemical Imagination at Work in Very Tight Places. *Angew. Chem., Int. Ed.* **2007**, *46*, 3620−3642.

(6) Pickard, C. J.; Needs, R. J. Highly compressed ammonia forms an ionic crystal. *Nat. Mater.* **2008**, *7*, 775−779.

(7) Zhao, Z.; Xu, B.; Tian, Y. Recent Advances in Superhard Materials. *Annu. Rev. Mater. Res.* **2016**, *46*, 383−406.

(8) Pickard, C. J.; Salamat, A.; Bojdys, M. J.; Needs, R. J.; McMillan, P. F. Carbon nitride frameworks and dense crystalline polymorphs. *Phys. Rev. B: Condens. Matter Mater. Phys.* **2016**, *94*, No. 094104.

(9) Peng, F.; Yao, Y.; Liu, H.; Ma, Y. Crystalline LiN_5 Predicted from First-Principles as a Possible High-Energy Material. *J. Phys. Chem. Lett.* **2015**, *6*, 2363−2366.

(10) Song, Y. New Perspectives on Potential Hydrogen Storage Materials Using High Pressure. *Phys. Chem. Chem. Phys.* **2013**, *15*, 14524−14547.

(11) Naumov, P.; Chizhik, S.; Panda, M. K.; Nath, N. K.; Boldyreva, E. Mechanically Responsive Molecular Crystals. *Chem. Rev.* **2015**, *115*, 12440−12490.

(12) Boldyreva, E. V. High-Pressure Diffraction Studies of Molecular Organic Solids. A Personal View. *Acta Crystallogr., Sect. A: Found. Crystallogr.* **2008**, *64*, 218−231.

(13) Katrusiak, A. High-Pressure Crystallography. *Acta Crystallogr., Sect. A: Found. Crystallogr.* **2008**, *64*, 135−148.

(14) Cai, W.; Gladysiak, A.; Aniola, M.; Smith, V. J.; Barbour, L. J.; Katrusiak, A. Giant Negative Area Compressibility Tunable in a Soft Porous Framework Material. *J. Am. Chem. Soc.* **2015**, *137*, 9296−9301.

(15) Lanza, A.; Germann, L. S.; Fisch, M.; Casati, N.; Macchi, P. Solid-State Reversible Nucleophilic Addition in a Highly Flexible MOF. *J. Am. Chem. Soc.* **2015**, *137*, 13072−13078.

(16) Andrzejewski, M.; Katrusiak, A. Piezochromic Topology Switch in a Coordination Polymer. *J. Phys. Chem. Lett.* **2017**, *8*, 929−935.

(17) Andrzejewski, M.; Katrusiak, A. Piezochromic Porous Metal-Organic Framework. *J. Phys. Chem. Lett.* **2017**, *8*, 279−284.

(18) Szafranski, M.; Katrusiak, A. Mechanism of Pressure-Induced Phase Transitions, Amorphization, and Absorption-Edge Shift in Photovoltaic Methylammonium Lead Iodide. *J. Phys. Chem. Lett.* **2016**, *7*, 3458−3466.

(19) Szafranski, M.; Katrusiak, A. Photovoltaic Hybrid Perovskites under Pressure. *J. Phys. Chem. Lett.* **2017**, *8*, 2496−2506.

(20) Minkov, V. S.; Boldyreva, E. V. Weak Hydrogen Bonds Formed by Thiol Groups in N-Acetyl-Cysteine and Their Response to the Crystal Structure Distortion on Increasing Pressure. *J. Phys. Chem. B* **2013**, *117*, 14247−14260.

(21) Boldyreva, E. Combined X-ray Diffraction and Raman Spectroscopy Studies of Phase Transitions in Crystalline Amino Acids at Low Temperatures and High Pressures: Selected Examples. *Phase Transitions* **2009**, *82*, 303−321.

(22) Fisch, M.; Lanza, A.; Macchi, P.; Casati, N. The Benefits of One-Dimensional Detectors for High-Pressure Powder X-ray Diffraction. *J. Appl. Crystallogr.* **2015**, *48*, 1956−1963.

(23) Patyk, E.; Skumiel, J.; Podsiadlo, M.; Katrusiak, A. High-Pressure (+)-Sucrose Polymorph. *Angew. Chem., Int. Ed.* **2012**, *51*, 2146−2150.

(24) Patyk, E.; Katrusiak, A. Transformable H-Bonds and Conformation in Compressed Glucose. *Chem. Sci.* **2015**, *6*, 1991−1995.

(25) Boldyreva, E.; Dera, P. *High-Pressure Crystallography, From Fundamental Phenomena to Technological Applications*; Springer, 2009.

(26) Casati, N.; Macchi, P.; Sironi, A. Molecular Crystals under High Pressure: Theoretical and Experimental Investigations of the Solid-Solid Phase Transitions in $[Co_2(CO)_6(XPh_3)_2]$(X = P, As). *Chem. - Eur. J.* **2009**, *15*, 4446−4457.

(27) Montisci, F.; Lanza, A.; Casati, N.; Macchi, P. NO_2NO_2 Contacts under Compression: Testing the Forces in Soft Donor-Acceptor Interactions. *Cryst. Growth Des.* **2018**, *18*, 7579−7589.

(28) Dziubek, K.; Podsiadlo, M.; Katrusiak, A. Nearly Isostructural Polymorphs of Ethynylbenzene: Resolution of CHπ(Arene) and Cooperative CHπ(C-C) Interactions by Pressure Freezing. *J. Am. Chem. Soc.* **2007**, *129*, 12620−12621.

(29) Tse, J. S.; Klug, D. D.; Patchkovskii, S.; Ma, Y.; Dewhurst, J. K. Chemical Bonding, Electron-Phonon Coupling, and Structural Transformations in High-Pressure Phases of Si. *J. Phys. Chem. B* **2006**, *110*, 3721−3726.

(30) Yamanaka, T.; Okada, T.; Nakamoto, Y. Electron Density Distribution and Static Dipole Moment of $KNbO_3$ at High Pressure. *Phys. Rev. B: Condens. Matter Mater. Phys.* **2009**, *80*, No. 094108.

(31) Fabbiani, F. P. A.; Dittrich, B.; Pulham, C. R.; Warren, J. E. Towards Charge-Density Analysis of High-Pressure Molecular Crystal Structures. *Acta Crystallogr., Sect. A: Found. Crystallogr.* **2011**, *67*, C376−C376.

(32) Macchi, P.; Casati, N. Strong Hydrogen Bonds in Crystals under High Pressure. *Acta Crystallogr., Sect. A: Found. Crystallogr.* **2011**, *67*, C163−C164.

(33) Casati, N.; Kleppe, A.; Jephcoat, A. P.; Macchi, P. Putting Pressure on Aromaticity along with In Situ Experimental Electron Density of a Molecular Crystal. *Nat. Commun.* **2016**, *7*, 10901.

(34) Casati, N.; Genoni, A.; Meyer, B.; Krawczuk, A.; Macchi, P. Exploring Charge Density Analysis in Crystals at High Pressure: Data Collection, Data Analysis and Advanced Modelling. *Acta Crystallogr., Sect. B: Struct. Sci., Cryst. Eng. Mater.* **2017**, *73*, 584−597.

(35) Pastorczak, E.; Corminboeuf, C. Perspective: Found in Translation: Quantum Chemical Tools for Grasping Non-Covalent Interactions. *J. Chem. Phys.* **2017**, *146*, 120901.

(36) Bader, R. F. W. *Atoms in Molecules: A Quantum Theory*; Oxford University Press, 1990.

DOI: 10.1021/acs.jpclett.9b00220
J. Phys. Chem. Lett. 2019, 10, 1482−1488

(37) Genoni, A.; Bucinsky, L.; Claiser, N.; Contreras-García, J.; Dittrich, B.; Dominiak, P. M.; Espinosa, E.; Gatti, C.; Giannozzi, P.; Gillet, J.-M.; et al. Quantum Crystallography: Current Developments and Future Perspectives. *Chem. - Eur. J.* **2018**, *24*, 10881−10905.
(38) Grabowsky, S.; Luger, P.; Buschmann, J.; Schneider, T.; Schirmeister, T.; Sobolev, A. N.; Jayatilaka, D. The Significance of Ionic Bonding in Sulfur Dioxide: Bond Orders from X-ray Diffraction Data. *Angew. Chem., Int. Ed.* **2012**, *51*, 6776−6779.
(39) Chęcińska, L.; Mebs, S.; Ośmia-lowski, B.; Zakrzewska, A.; Ejsmont, K.; Kohout, M. Tuning the Electronic Properties of the Dative NB Bond with Associated OB Interaction: Electron Localizability Indicator from X-Ray Wavefunction Refinement. *ChemPhysChem* **2016**, *17*, 2395−2406.
(40) Saleh, G.; Gatti, C.; LoPresti, L.; Contreras-García, J. Revealing Non-covalent Interactions in Molecular Crystals through Their Experimental Electron Densities. *Chem. - Eur. J.* **2012**, *18*, 15523−15536.
(41) de Silva, P.; Corminboeuf, C. Simultaneous Visualization of Covalent and Noncovalent Interactions Using Regions of Density Overlap. *J. Chem. Theory Comput.* **2014**, *10*, 3745−3756.
(42) de Silva, P.; Korchowiec, J.; Wesolowski, T. A. Atomic Shell Structure from the Single-Exponential Decay Detector. *J. Chem. Phys.* **2014**, *140*, 164301.
(43) Vannay, L.; Meyer, B.; Petraglia, R.; Sforazzini, G.; Ceriotti, M.; Corminboeuf, C. Analyzing Fluxional Molecules Using DORI. *J. Chem. Theory Comput.* **2018**, *14*, 2370−2379.
(44) Marx, D.; Savin, A. Topological Bifurcation Analysis: Electronic Structure of CH. *Angew. Chem., Int. Ed. Engl.* **1997**, *36*, 2077−2080.
(45) Savin, A.; Silvi, B.; Colonna, F. Topological Analysis of the Electron Localization Function Applied to Delocalized Bonds. *Can. J. Chem.* **1996**, *74*, 1088−1096.
(46) Poater, J.; Duran, M.; Sola, M.; Silvi, B. Theoretical Evaluation of Electron Delocalization in Aromatic Molecules by Means of Atoms in Molecules (AIM) and Electron Localization Function (ELF) Topological Approaches. *Chem. Rev.* **2005**, *105*, 3911−3947.
(47) Piquemal, J.-P.; Pilme, J.; Parisel, O.; Gerard, H.; Fourre, I.; Berges, J.; Gourlaouen, C.; De La Lande, A.; Van Severen, M.-C.; Silvi, B. What Can Be Learnt on Biologically Relevant Systems from the Topological Analysis of the Electron Localization Function? *Int. J. Quantum Chem.* **2008**, *108*, 1951−1969.
(48) Mace, A.; Barthel, S.; Smit, B. Automated Multiscale Approach To Predict Self-Diffusion from a Potential Energy Field. *J. Chem. Theory Comput.* **2019**, DOI: 10.1021/acs.jctc.8b01255.
(49) Destro, R.; Pilati, T.; Simonetta, M. Another Aromaticity vs Non-Aromaticity Dilemma: The Structure of Anti-1,6:8,13-biscarbonyl[14]annulene. *Tetrahedron* **1980**, *36*, 3301−3304.
(50) Destro, R.; Merati, F. Bond Lengths, and Beyond. *Acta Crystallogr., Sect. B: Struct. Sci.* **1995**, *51*, 559−570.
(51) Bader, R. F.; Stephens, M. E. Spatial Localization of the Electronic Pair and Number Distributions in Molecules. *J. Am. Chem. Soc.* **1975**, *97*, 7391−7399.
(52) Stoll, H.; Wagenblast, G.; Preuss, H. On the Use of Local Basis Sets for Localized Molecular Orbitals. *Theor. Chim. Acta* **1980**, *57*, 169−178.
(53) Boldyreva, E. V. High-Pressure Studies of the Hydrogen Bond Networks in Molecular Crystals. *J. Mol. Struct.* **2004**, *700*, 151−155.
(54) Fanetti, S.; Citroni, M.; Bini, R. Pressure-Induced Fluorescence of Pyridine. *J. Phys. Chem. B* **2011**, *115*, 12051−12058.
(55) Fanetti, S.; Citroni, M.; Bini, R. Tuning the Aromaticity of *s*-Triazine in the Crystal Phase by Pressure. *J. Phys. Chem. C* **2014**, *118*, 13764−13768.
(56) Casati, N.; Macchi, P.; Sironi, A. Hydrogen Migration in Oxalic Acid Di-Hydrate at High Pressure? *Chem. Commun.* **2009**, *0*, 2679−2681.
(57) Boldyreva, E. V. High-Pressure Studies of the Anisotropy of Structural Distortion of Molecular Crystals. *J. Mol. Struct.* **2003**, *647*, 159−179.

DOI: 10.1021/acs.jpclett.9b00220
J. Phys. Chem. Lett. 2019, 10, 1482−1488